# Supplement to "Turbulent Dynamics of Buoyant Melt Plumes Adjacent Near-Vertical Glacier Ice"

### S1 Assessing the Structure of the Thermal Boundary Layer

Eight fast-response thermistors distributed along the thermistor rake (or T-rake) and three RBR-solos create a timeseries of $T$ at 11 locations that are used to image the turbulent near-boundary flow and to characterize scales of time-averaged temperature. On the T-rake, the thermistors (1.65 mm diameter, epoxy-encased Amphenol 10 kOhm 527-MC65F103B) are directly exposed to seawater and protrude out the side of a 4-mm carbon fiber tube with a goal of sampling the mean and fluctuating turbulent $T$ with minimal contamination. Thermistors were mounted at distances of 2, 4, 7, 12, 23, 39, 58 and 84 mm from the tube's tip (Fig. S1), and the sensors were oriented downward in anticipation of the mean buoyant flow being positive vertical. The roughly logarithmic spacing was chosen because of our expectation that temperature gradients increase with proximity to the boundary.

The thermistors were sampled at 100 Hz using 16-bit electronics adapted from Moum and Nash (2009) yielding 0.5 mK precision and $< 2$ mK accuracy over the calibrated $0-10$ C range. A $1/e$ time constant ($\tau = 0.2$ sec) was measured during dip tests in the lab; in the field their response was slower ($\tau \sim 1$ sec), likely due to thermal mass effects associated with their mounting configuration.

We attempted to deploy the Meltstake so that the thermistor rake was approximately perpendicular to the ice face, and as close to the ice as possible. At times, we believe the T-rake was in contact with the ice immediately following a drilling / Meltstake advance sequence. One challenge with these measurements is determining the distance between ice and T-rake tip ($y_o$), as this was not measured independently. In this section, we show how the various functional forms for the mean temperature structure are related, and in doing so, also outline our procedure for estimating the T-rake location ($y_o$, its distance from the ice).

There are no previous measurements of temperature in the boundary layer adjacent a rough, melting, near-vertical ice interface. Here we start with the similarity solution of Eckert and Jackson (1950) which was effective in describing the velocity structure of the plumes (Fig. 3). While it was initially derived for aerospace applications (and $Pr = 1$), it also provides an empirical

30 form for the temperature profile (their equation 4 and figure 2):

$$\theta = \theta_w \left[ 1 - \left( \frac{y}{\delta} \right)^{1/7} \right] \tag{S1}$$

31 where $\theta$ is the temperature anomaly associated with the plume, $\theta_w$ is the temperature difference

32 between wall and outer flow, and $\delta$ is the boundary layer thickness. However, this form (and the

33 data on which it was based) used air for the fluid and assumed the Prandtl number equals one.

34 As a result, the boundary layer thickness (that governs the decay scale) for $\theta$ is the same as that

35 for $w$ ($\delta$ and $L_w = 0.304\delta$). While it has been applied to the ice-ocean boundary to interpret

36 numerical simulations (Parker et al., 2021; Zhao et al., 2024), it is not expected to adequately rep-

37 resent the flow very near the ice, which differs from the assumed setting in at least two ways: (1)

38 from a diffusivity standpoint (the molecular diffusivities for heat $D_T$ and salt $D_S$ are 10-1000

39 times smaller than the molecular viscosity $\nu$), and (2) because of the possibility that ice-roughness

40 may strongly modify the near-boundary flow. As a result, we hypothesize that their form will be

41 most relevant far from the boundary, and consider a slightly modified version of equation (S1)

42 to describe the outer layer. We define:

$$\widehat{T} = T_a - \Delta T \left[ 1 - \left( \frac{y}{\delta} \right)^{1/7} \right], \tag{S2}$$



**Figure S1.** Configuration of thermistors on the T-rake; calipers provide scale. All 16 electrical leads are fed through the carbon tube, within which they transition to larger diameter copper wire; the entire assembly is then filled with a low-viscosity polyurethane adhesive to make the assembly waterproof. Newer versions of the T-rake have the Amphenol 527-MC65F103B sensing elements offset from the carbon tube an additional 3mm to provide better exposure to the turbulent flow. The thermistors in that configuration are supported by adhesive-filled heat-shrink tubing, which provides mechanical support, insulates the electrical leads, and thermally isolates the sensors from the carbon support tube.

in which $\delta$ is the same as Eckert and Jackson (1950)'s $\delta$ and computed by fitting $\widehat{w}$ to the vertical velocity profile (equation (1)). We introduce $\Delta T$ to represent the temperature drop through the outer (turbulence dominated) boundary layer, but not including the inner, diffusive layer over which the temperature drops to freezing, and where differences between $D_T$, $D_S$ and $\nu$ will be most important. In Eckert and Jackson (1950)'s original form, there is no $\Delta T$: $\Delta T$ was set to equal $T_a$ in order for $\widehat{T}$ to reach $0°$ C at the boundary. However, if we use their form and set $\Delta T = T_a$, the predicted temperature is far too diffuse (and colder) than that observed. We demonstrate this in the upper panels of figure S2, where the thin dotted lines are $\widehat{T} = T_a - T_a(1 - (y/\delta)^{1/7})$. Hence, the lengthscale $L_w$ (and $\delta$) derived from our fits of $\widehat{w}$ to $w$ does not characterize total temperature drop from ambient ($T_a$) to ice assuming this functional form.

Here we recognize that Eckert and Jackson (1950)'s Prandtl number assumption ($Pr = 1$) is not expected to be valid here, and especially near the ice interface where molecular processes (and differences between $D_T$ and $\nu$) control transports across the viscous sublayer. In this region, we should not expect $\delta$ – the scale derived from $w(y)$ and associated with momentum transports by the turbulent stress – to be appropriate. For this reason we introduce a second length scale, $L_T$, relevant to $T(y)$ as $y \to 0$, used to characterized the inner sublayer that results from an interplay between molecular and turbulent processes that diffuses the buoyant meltwater and its thermal signature. We envision this sublayer as a way of connecting the outer boundary layer region – controlled by plume turbulence and described by eq. (S2) and $\delta$ – to the boundary, so that only a small fraction of the temperature drop occurs in the outer region (as we observe). For this reason we introduced $\Delta T$ in eq. S2 and perform a least-squares minimization to the outer 5 temperature measurements. We find (fig. S2) that $T$ in the outer boundary layer is approximately represented by this model (heavy dotted lines). From these fits, $\Delta T \sim 1°$ in each case, which corresponds to a 0.2-0.3 °C temperature drop in the outer boundary layer where the model best represents the data.
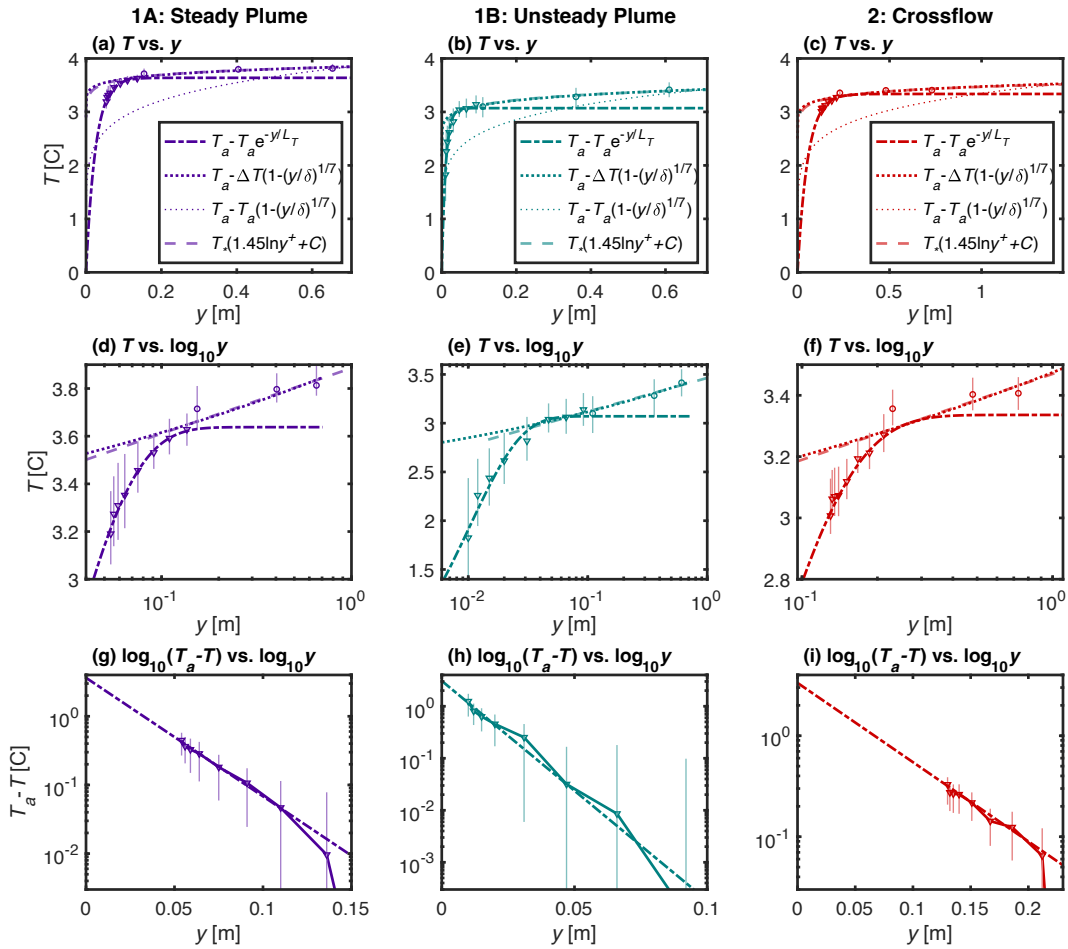
In this hybrid model, most of the temperature drop must occur within the inner boundary layer, for which we propose $T$ approximately follows an exponential function of the form

$$\widehat{T}(y) = T_a - (T_a - T_i)e^{-y/L_T}. \tag{S3}$$

Here, $T_a$ is the ambient (farfield) temperature and $T_i$ is the water temperature on the ocean side of the ice interface, and $L_T$ is a thermal-diffusive lengthscale. We note that laboratory experiments (Josberger & Martin, 1981; McConnochie & Kerr, 2017) suggest that $T_i = -0.5°$C; how-

73 ever, to simplify equation S3, we assume $T_i = 0°$ C (equal to the ice temperature); this assump-

74 tion has little effect on our results. To determine $T_a$, $L_T$ and $y_o$ (the offset of the T-rake from the

75 ice), we minimize $\sum_{n=1}^{8} (T(y_n) - \widehat{T}(y_n))^2$ for each of the $n$ thermistors, with $y_n = y_o + y'_n$,

76 where $y'_n$ is the location of each sensor relative to the T-rake tip[1]. In the present configuration

77 of the Meltstate, the T-rake is at a fixed location relative to the iceberg, and as a result, as the ice

---

[1] We determine fits to the data by minimizing the squared residual between model and data using the Levenberg-Marquardt nonlinear least squares algorithm as implemented in Matlab's nlinfit.m (Seber & Wild, 2003).



**Figure S2.** Mean character of the observed thermal boundary layer. Data are the same as in fig. 3c, but separated into the three individual periods: Case 1A: 29-May-2023 20:40-21:00 (a,d,g); Case 1B: 29-May-2023 23:06:45-23:26:45 (b,e,h); and Case 2: 30-May-2023 01:48-02:05 (c,f,i). Each row presents the data with different axes (linear-linear, linear-log, and log-log) to highlight the character of each layer and corresponding fit. The dash-dot lines represent fits in the inner sublayer (equation S3), the heavy dotted lines represent the fit to the modified Eckert and Jackson (1950) form (equation S2), and the light dotted lines are Eckert and Jackson (1950)'s original form (equation S1).

| | Outer boundary layer Eckert & Jackson (1950) | | | Inner boundary layer Exponential fit | | | Transition Distance |
|---|---|---|---|---|---|---|---|
| Case | $T_a$ [°C] | $\Delta T$ [°C] | $\delta$ [cm] | $T_a$ [°C] | $L_T$ [cm] | $y_o$ [cm] | $L_{out}$ [cm] |
| 1A | 3.85 | 0.95 | 70 | 3.64 | 2.5 | 5.4 | 1.5 |
| 1B | 3.42 | 1.25 | 71 | 3.07 | 1.0 | 1.0 | 2.1 |
| 1B (10 min) | | | | 3.12 | 0.8 | 0.5 | |
| 1B (5 min) | | | | 3.0 | 0.6 | 0.2 | |
| 2 | 3.53 | 1.02 | 144 | 3.34 | 5.5 | 13 | 3.2 |

**Table S1.** Coefficients for empirical forms presented in Fig. S2. Case 1B (10 min) and (5 min) represents the coefficients computed from the first 10 and 5 minutes respectively. $L_{out}$ is the distance at which $y^+ = 30$, and represents the outer scale of the transition layer and a measure of the maximum extent of viscous boundary effects.

melts, $y_o$ increases in time. For this reason, we choose relatively short (20 min) periods for these calculations, and assume $y_o$ is constant over each period.

For completeness, we also include a formulation for the boundary layer's thermal structure presented in Tsuji and Nagano (1988) that relaxes the assumption of $Pr = 1$. Here we follow their conventions and define the dimensionless distance from the wall as $y^+ = u_* y / \nu$, where $u_* = \sqrt{\tau_w / \rho}$ is the friction velocity that is derived from equation (4) using our fit to the vertical velocity profile. Hence, $y^+$ is based on the momentum scaling. They also define the dimensionless temperature $T^+ = (T - T_i)/T_*$ where $T_*$ is the "friction temperature" and $T_i$ is the temperature at the wall. Their formation also breaks the boundary layer into two sub-regions: (1) a viscous sublayer very close to the wall (valid for distances $0 < y^+ < 5$), where $T$ varies linearly with $y$ such that $T^+ = Pr y^+$, and (2) an outer turbulent layer (valid for distances of $30 < y^+ < 200$), for which

$$T^+ = 1.45 \ln y^+ + C. \tag{S4}$$

We apply this equation to our observations by fitting equation S4 to data from the outer five sensors[1]. In their formulation there is a transition layer between these two regions ($5 < y^+ < 30$), which depends on details of flow development (and the Grashof number), which we do not investigate here. However, because of the importance of $y^+$ in delineating the inner and outer boundary layers, we define $L_{out} = 30\nu/u_*$ as the distance where the outer (turbulence-dominated) boundary layer dynamics are at play. We also note that Tsuji and Nagano (1988) found experimental agreement primarily within the inner sublayer; significant deviation was observed when comparing equation S4 to experimental observations of the outer boundary layer. We note, however, that few data were acquired in an aquatic environment.

To demonstrate the differences in boundary layer shapes, we present each of these fits in figure S2. We present the same data (and fits) on three separate plots using different axes (linear-linear, linear-log, and log-log) to highlight the shape of each function and its relation to the data in the two different boundary layer regions. The upper two rows of plots show how the outer sensors are well represented by our modified version of Eckert and Jackson (1950)'s model and equation (S2). Our data are also consistent with Tsuji and Nagano (1988)'s formulation, which is largely indistinguishable from Eckert and Jackson (1950)'s in the outer layer. In contrast, the inner boundary layer closely follows the exponential form presented in equation (S3), which is highlighted in the bottom rows. We find that the inner plume thermal-diffusive lengthscales ($L_T = 1 - 4$ cm) are a factor of ten smaller than $L_w$ (= $25 - 50$ cm), and that both scales are largest during periods of strong crossflow (case 2).

Note that in case 1B (in particular), the T-rake was very close to the ice, so the change in $y_o$ over the 20 min period during which the mean is computed turns out to be an appreciable fraction of $y_o$. Because of this, we also perform the exponential fit calculations using shorter subsets of the data (the first 5- and 10-min) that correspond to the subsets of data presented in Figure 3. During this time, we find that $y_o$ increases monotonically, such that $y_o = 2$ mm when computed over the first 5-min period, $y_o = 5$ mm when computed over the first 10 min, and $y_o = 10$ mm when computed over the entire 20 min. Thus, the innermost T-rake thermistor was on average 4 mm from the ice during the first five minutes, increasing to 7 mm over the next five minutes. That sensor recorded $0°$ C during three meltwater ejection events, each separated $\sim$100 seconds in time. During these first 5-min, the temperature decay scale was $L_T = 6$ mm, slightly smaller than the 20-min average ($L_T = 10$ mm). A summary of all fits is shown in Table S1.

## References

Eckert, E. R. G., & Jackson, T. W. (1950). Analysis of turbulent free-convection boundary layer on flat plate. *National Advisory Committee on Aeronautics*, *Technical Note 2207*.

Josberger, E. G., & Martin, S. (1981). A laboratory and theoretical study of the boundary layer adjacent to a vertical melting ice wall in salt water. *Journal of Fluid Mechanics*, *111*, 439–473.

McConnochie, C. D., & Kerr, R. C. (2017). Enhanced ablation of a vertical ice wall due to an external freshwater plume. *Journal of Fluid Mechanics*, *810*, 429–447.

Moum, J. N., & Nash, J. D. (2009). Mixing measurements on an Equatorial ocean mooring.

*Journal of Atmospheric and Oceanic Technology*, *26*, 317–336.

Parker, D., Burridge, H., Partridge, J., & Linden, P.   (2021).   Vertically distributed wall sources of buoyancy. Part 1. Unconfined. *Journal of Fluid Mechanics*, *907*, A15.

Seber, G. A., & Wild, C. J.   (2003).   Nonlinear regression.   *New Jersey: John Wiley & Sons*, *62*(63), 1238.

Tsuji, T., & Nagano, Y.   (1988).   Characteristics of a turbulent natural convection boundary layer along a vertical flat plate.   *International journal of heat and mass transfer*, *31*(8), 1723–1734.

Zhao, K., Skyllingstad, E., & Nash, J.   (2024).   Improved parameterizations of vertical ice-ocean boundary layers and melt rates. *Gephys. Res. Lett*, *in press*.